Science of the Total Environment 954 (2024) 176564

Contents lists available at ScienceDirect

Science of the Total Environment

journal homepage: www.elsevier.com/locate/scitotenv

Manganese(III) dominants the mobilization of phosphorus in reducing sediments: Evidence from Aha reservoir, Southwest China

Quan Chen [a,b,f], Jing-fu Wang [a,b,f,*], Meng-qiang Zhu [c], Hai-bo Qin [a,b], Peng Liao [a,b,f], Zhi-tong Lu [b,d], Peng-cheng Ju [e], Jing-an Chen [a,b,f,*]

[a] State Key Laboratory of Environmental Geochemistry, Institute of Geochemistry, Chinese Academy of Sciences, Guiyang 550081, China
[b] University of Chinese Academy of Sciences, Beijing 100049, China
[c] Department of Geology, University of Maryland, College Park, MD 20740, USA
[d] State Key Laboratory of Ore Deposit Geochemistry, Chinese Academy of Sciences, Institute of Geochemistry, Guiyang 550081, China
[e] State Key Laboratory of Continental Dynamics and Shaanxi Key Laboratory of Early Life and Environment, Department of Geology, Northwest University, Xi'an 710069, China
[f] Guizhou Province Field Scientific Observation and Research Station of Hongfeng Lake Reservoir Ecosystem, Guiyang 551499, China

HIGHLIGHTS

- Couple cycle between Mn and P were observed in reducing sediments.
- P mobilization in reducing sediments was mainly driven by Mn(III).
- Fe mainly deposited as inert Fe minerals leads the decoupled of P and Fe.
- Updated P cycle patterns in different sedimentary environments were proposed.

GRAPHICAL ABSTRACT

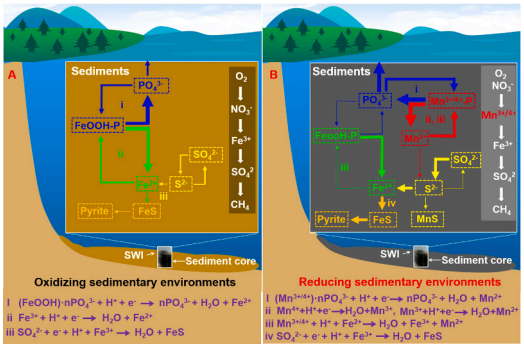

ARTICLE INFO

Editor: Bo Gao

Keywords:
Phosphorus
Mobilization mechanism
Manganese(III)
Reducing sediments
Eutrophication

ABSTRACT

Eutrophication has become one of the greatest threats to aquatic ecosystems. The release of phosphorus (P) from sediments exerts a critical role on eutrophication level. Both manganese (Mn) and iron (Fe), sensitive to redox conditions, own strong affinity for P. Numerous works have demonstrated that Fe was a key factor to drive P cycle in sediments. However, the role of Mn on P mobilization remains largely unexplored. Herein, the mechanism of P mobilization driven by Mn were investigated in a seasonal anoxic reservoir. Diffusive gradients in thin films (DGT) results, from both field investigations and laboratory incubations, showed P was synchronously distributed and significantly positive correlated ($r^2 \geq 0.40$, $p < 0.01$) with Mn, suggested that P cycle was associated with Mn. X-ray photoelectron spectroscopy (XPS) results showed that in the outer layers at the top 1 cm sediment pellet the contents of Mn and P occurred significantly synchronize changed, while that of Fe remains virtually unchanged when oxygen conditions changed. This demonstrated that Mn is likely to be the key

* Corresponding authors at: State Key Laboratory of Environmental Geochemistry, Institute of Geochemistry, Chinese Academy of Sciences, Guiyang 550081, China.
E-mail addresses: wangjingfu@vip.skleg.cn (J.-f. Wang), chenjingan@vip.skleg.cn (J.-a. Chen).

https://doi.org/10.1016/j.scitotenv.2024.176564
Received 27 May 2024; Received in revised form 20 August 2024; Accepted 25 September 2024
Available online 27 September 2024

factor affect P cycle. Most importantly, the relative content of Mn(III) changed the most (≈20 %) interpreted that Mn(III) is the key Mn species dominants the P mobilization. Furthermore, Dual-Beam scanning electron microscope (DB-SEM) maps clearly showed the co-enrichment of P and Mn in oxic sediments, confirmed P was mainly hosted by Mn minerals. In contrast, the random distributions and weak or negative correlations between P and Fe implied that P cycle was decouple with Fe, this resulted from that Fe was almost deposited as inert Fe fractions (>99.2 %) in reducing sediments. This study significantly expanded our knowledge on the geochemical behavior of P influenced by Mn in aquatic sediments.

1. Introduction

Phosphorus (P) is an essential element in setting primary productivity in aquatic ecosystems (Tyrrell, 1999; Kipp and Stüeken, 2017; Duhamel et al., 2021). Eutrophication, partially was triggered by the over loading of P, is widely acknowledged as one of the most severe issues in aquatic ecosystems (Conley et al., 2009; Tong et al., 2017; Maure et al., 2021). Since 1950, the deposition of P in aquatic sediments has accelerated due to fertilization, industrial pollution emissions, and the bloom of dam constructions (Maavara et al., 2020; Rodriguez et al., 2020; Zhu et al., 2020). As a result, eutrophication in surface waters and coastal ecosystems have been detonated due to the release of these deposited P (Maavara et al., 2015; Powers et al., 2016; Rodriguez et al., 2020). Dissolved orthophosphates, which can be used directly by organisms, readily bind to metal (hydroxyl) oxides in the water column and thus precipitate into the sediments (Paytan and McLaughlin, 2007). Metal-bound P can potentially be remobilized and diffused back into the overlying water under anoxic conditions, thus lengthening its residence time in the water column and bolstering nutrient availability for primary productivity (Ingall and Jahnke, 1994; Rousselaki et al., 2024). This transfer of P is believed to be responsible for the elevated eutrophication in aquatic ecosystems (Alcott et al., 2019; Dadi et al., 2023). Hence, comprehending the cycle and mechanisms of metal (hydroxyl) oxide-bound P is critical for effective governing eutrophication.

Numerous studies have focused on the effects of iron (Fe) on the P cycle (Konhauser et al., 2007a; Zerkle et al., 2012; Xiong et al., 2019, 2023). Especially, the aquatic ecosystems of early Earth were abundant in dissolved divalent Fe, it was only after the emergence of photosynthetic autotrophic microorganisms that the Earth's oxidation and subsequent conversion of Fe(II) to Fe(III) occurred accompanied by the co-precipitation and adsorption of P (Walton et al., 2023). Besides, depending on the decomposition rate of organic materials and Fe reduction, P may be released back into the water column (Kipp and Stüeken, 2017; Xiong et al., 2019). This release of P could be elevated by the formation of sulfides in sediments, as well as by the reductive dissolution of Fe (oxyhydr)oxide minerals by hydrogen sulfide (Poulton, 2003; Poulton et al., 2004; Wu et al., 2019). A significant turning point occurred after the Great Oxidation Event, which led to the rapid depletion of dissolved Fe from aquatic ecosystems (Bjerrum and Canfield, 2002; Konhauser et al., 2007b; Jones et al., 2015), and caused significant burial of P. Those P burial offered opportunities for other non-Fe metals like manganese (Mn) involvement in the cycle of P. However, little attentions were given to the role of non-Fe metals in the mobilizing of P in sediments, resulting in a scarce understanding to their underlying mechanisms.

Consistent with Fe, Mn also has soluble reduced forms and insoluble oxyhydroxides that are readily interconvert near the redox boundary (Davison, 1993; Ming et al., 2024). Especially the three valence states (II, III, and IV) of Mn are highly sensitive to the changes of redox conditions (Madison et al., 2013; Wang et al., 2024). Previous kinetic studies have illuminated that the oxidation rate of Mn^{2+} by molecular O_2 is 2–6 orders of magnitude slower than that of Fe^{2+} (Davison, 1993). Besides, the solubility of FeS is significantly lower compared with that of MnS [$K_{sp}(FeS) = 6.3 \times 10^{-18}$ versus $K_{sp}(MnS) = 2.5 \times 10^{-13}$], this would result in more Mn could be geochemical cycled again when redox conditions changed in sediments. Especially if Fe was deposited as inert minerals (e.g. FeS) in the inner layer of sediment pellets, the oxidation of Mn^{2+} could lead to Mn (oxy)hydroxides complexed with P and coated on the pellet surface (Davison, 1993; Ji et al., 2022). Those above processes could lead Mn become a key factor for P mobilization (Dodd et al., 2023). Although the role of Mn on the mobilization of P in sediments were mentioned by some studies (Schroth et al., 2015; Hermans et al., 2019; Pan et al., 2019; Li et al., 2021; Zhou et al., 2024). However, the specific mechanism of P mobilization driven by Mn redox in sediments remains unclear.

Based on the difference in redox processes between Fe and Mn, we proposed a mechanism for the mobilization of P driven by Mn redox in sediments: P is mainly complexed with Mn oxides to form Mn-bond P and coated on the sediments pellet surface under oxic conditions, then the rapid reduction of Mn-bond P lead the simultaneous mobilization of P and Mn under anoxic conditions. To test this hypothesis, we selected a seasonal hypoxic reservoir with reducing sedimentary conditions, sediment cores covered oxic and anoxic seasons were collected to characterize P fractions, and indoor incubation were conducted to investigate the underlying mechanisms of P mobilization. The objectives of this study were (1) to investigate the geochemical behavior of P, Mn, Fe and S by their distributions in sediments and (2) to interpret the specific mechanism of P mobilization driven by Mn. This study is expected to illuminate how Mn controls the mobilization of P, offering novel insights into the geochemical cycle of P in aquatic sediments.

2. Materials and methods

2.1. Study area and sample site

Aha reservoir (26°30′-26°34′ N, 106°37′-106°40′ E), was constructed in 1960, is one of the oldest reservoirs in China (Fig. S2), which is a valley-type reservoir and has a maximum and average depth of 29 m and 13 m respectively. After over 60 years in operation, pollution of P in Aha reservoir is severe due to persistent external input from point and non-point sources (Chen et al., 2018). Aha reservoir also experienced regional harmful algal blooms over the past two decades despite external P inputs were well governed (Chen et al., 2018). Besides, the constant inflow of runoff and sewage from Aha watershed has resulted in the contamination of its sediments with Fe and Mn (Song et al., 2011; Yang et al., 2022). To date, Aha reservoir has grown to be a seasonally stratified reservoir with its hypolimnion usually exposed under anoxic conditions (<2 mg L^{-1}) during summer and autumn (Fig. S3). Additionally, Aha reservoir is operating in a relatively stable system due to dam is its only outlet and only discharge water once a year in late spring. As such, sedimentary environments in Aha has grown to be a reducing condition after the intensive biogeochemical modification (Ma and Banfield, 2011; Kang et al., 2018). In summary, the dam zone was selected as the study site because it reflected the overall contamination level in Aha reservoir, which is more conducive to revealing the mobilization mechanism of P.

2.2. Field investigation and analyses

Seasonal field investigations were conducted in January, April, July, and October in 2020. Duplicate intact sediment cores with a 10–20 cm overlying water layer were retrieved using a gravity sampler (length ×

diameter = 50 cm × 12 cm). A rubber stopper was used to seal the bottom of sediment core. Because diffusive gradients in thin films technique (DGT) owns the advantage of accurately pre-concentrate labile species in sediments (Davison and Zhang, 1994; Ding et al., 2016a). So, a flat-type DGT device (ZrO-CA DGT, see detail description of DGT in Text S1), comprising binding gel and diffusion layer, was selected for in-situ sampling. The DGT probe was inserted into the sediment core vertically for minimally reduced physical disturbance to the sediment core (Ding et al., 2016b). Furthermore, a 2–4 cm long DGT probe was remained in overlying water to sample sulfide (S(-II)), P(V), Mn(II), and Fe(II). Then, the core with DGT probe was fixed on a self-developed tripod lander and the lander was placed back to the reservoir bottom slowly with a nylon rope (Fig. S4). Finally, a multi-parameter water quality monitor (YSI 6600-V2, YSI Inc., Yellow Springs, USA), calibrated with standard solutions, was used to determine the depth profile of O_2 concentrations in water column at a resolution of 1 m.

The ZrO-CA DGT was utilized to sample P(V), Mn(II), Fe(II), and S(-II) simultaneously in sediment porewater (Ding et al., 2016b; Wang et al., 2016; Wang et al., 2019b). Aqueous ions of S(-II), P(V), Mn(II), and Fe(II) were captured by binding gel after passing the diffusion layer from the exposure window (length × width = 15 cm × 1.8 cm). The DGT probe was deployed in the field for 24 h to ensure that the binding gel could enrich enough mass to exceed the limit of lowest detection. After retrieving the DGT probe, the probe surface was cleaned by ultrapure water (resistivity: 18.2 MΩ cm, Milli-Q, Millipore) to remove adsorbed sediments particles completely. Then the cleaned probe was wrapped by aluminum foil after adding a few drops of ultrapure water to keep a moisturized environment, and was then stored in a 4 °C portable refrigerator and brought back to the laboratory for chemical analyses.

Chemical analyses of DGT gel were followed the methods reported by Ding et al. (2010, 2012). Briefly, DGT-S(-II) concentrations were firstly determined by computer-imaging densitometry (CID) technique. Then, a ceramic knife was used to cut the exposure window zone to take out the binding gel, which was then cut into long strips (length × width = 18.0 mm × 2.0 mm) at 2.0 mm intervals along the sediment vertical profile using the ceramic slicing knife. The DGT gel strip was transferred into a 1.5 mL centrifuge tube and 1 M HNO_3 was added to extract both DGT-Fe(II) and DGT-Mn(II). Subsequently, the DGT gel strip was moved to a new 1.5 mL centrifuge tube and 1 M NaOH was added for DGT-P(V) extraction (Wang et al., 2016, 2017). Both extraction steps were conducted at the room temperature (25 ± 3 °C). The extraction time for DGT-P(V) was 16 h and that for DGT-Fe(II)/DGT-Mn(II) was 24 h (Wang et al., 2017). The concentration of DGT-P(V) was determined by a miniaturized molybdenum blue and phenanthroline colorimetric method (Xu et al., 2013), and the concentrations of DGT-Fe(II)/DGT-Mn(II) were determined by inductively coupled plasma mass spectrometer (ICP-MS, Agilent Technologies 7700×, USA).

2.3. Laboratory incubation experiment and analyses

To better investigate the micro-mechanism of Mn-driven P mobilization, four sediment cores were collected from the field study site in winter for laboratory incubation experiments (Fig. S5). The first two cores were operated under oxic conditions (O_2 concentrations >6 mg L^{-1}) by venting O_2 into the overlying water intermittently, and the subsequent two cores were incubated under anoxic conditions (O_2 concentrations <2 mg L^{-1}) by a continued ventilation of pure N_2 (purity >99.99 %). The incubation time was 15 days. To ensure stable redox conditions during incubation experiments, the O_2 concentrations in the overlying water were measured using a multi-parameter water quality monitor with a frequency of three times a day (at 8:00 am, 14:00 pm, and 22:00 pm). Roughly 20-mL of overlying water was sampled daily to determine TP, SRP, Fe, Mn, and SO_4^{2-} concentrations. Meanwhile, DGT sampling was also performed in laboratory incubation experiment. On day-14, the ZrO-CA DGT probe was inserted into sediment cores and retrieved on day-15. After retrieving the DGT probe, the top 10 cm sediment from four sediment cores were sectioned at a 1 cm resolution in a N_2-purged glovebox. Sediment samples were stored in 50 mL centrifuge tubes and lyophilized at −70 °C. Finally, half of the lyophilized sediments were ground to 200 mesh for further chemical analyses.

The DGT analyses for laboratory incubation experiments were similar to those presented in the field investigation (shown above). Besides, half of overlying water samples without filtration were directly used to determine total P (TP), total Fe, and total Mn concentrations. The remaining half was filtered through a 0.45 μm filter to determine the soluble reactive phosphate (SRP) and sulfate (SO_4^{2-}) concentrations. The sedimentary P fractions were determined by the Sequential P extraction procedures presented by Hupfer et al. (1995). The solid-phase P was operationally defined as (1) NH_4Cl-extracted P (NH_4Cl-P), (2) bicarbonate/dithionite-extracted P (BD-P), (3) NaOH-extracted P (NaOH-P), (4) HCl-extracted P (HCl-P), and (5) organic and other refractory P (Residual-P). Fe and Mn fractions in sediments were determined by the modified Community Bureau of Reference (BCR) sequential extraction procedure (Nemati et al., 2011). For the extracted solutions and overlying water of sediment cores, P concentrations were determined by molybdenum blue method (Murphy and Riley, 1962), the Fe/Mn concentrations were determined by the ICP-MS (Agilent Technologies 7700×, USA). The SO_4^{2-} concentrations were determined by ion chromatograph (DIONEX ICS-90, USA).

The lyophilized un-ground samples collected at the top 1 cm sediment were characterized by spectroscopic and microscopic techniques. Briefly, X-ray photoelectron spectroscopy (XPS; PHI 5000 Versaprobe III, ULVAC-PHI, Japan) was used to conduct depth-profile analyses for valence states and compositions of C, P, Fe, and Mn in sediment pellets. XPS spectra were processed using PHI MultiPak software (version 9.8). Fe mineral phases were characterized by ^{57}Fe Mössbauer spectroscopy at 13 K (Williams and Scherer, 2004). The collected Mössbauer data were fitted with MossWinn software (Version 4.0 Pre) using Lorentzian line shape (Williams and Scherer, 2004). In addition, high-resolution elemental maps of Mn, Fe, and P were obtained by the FEI Scios Dual-Beam scanning electron microscope (DB-SEM) equipped with the energy-dispersive X-ray spectroscopy (EDS) located in the Institute of Geochemistry, Chinese Academy of Sciences. Fe/Mn K-edge XANES bulk spectra of the top 1 cm sediments samples were collected at the BL14W1 beamline that equipped with a Si(111) double-crystal monochromator at the Shanghai Synchrotron Radiation Facility (SSRF, Shanghai, China). Fe/Mn reference materials were measured in transmission mode, while the samples were placed at an angle of 45° from the incident beam and measured in fluorescence mode by using a 19-element Ge solid-state detector under ambient conditions. XANES data analyses were performed in ATHENA (Ravel and Newville, 2005). The background was removed from the raw XANES spectra by a spline smoothing method (Qin et al., 2017). Linear combination fittings (LCF) for the XANES spectra were conducted as previously described to obtain Fe and Mn speciation quantitatively (Qin et al., 2021). The quality of XANES simulation were evaluated by the goodness of fit parameter, R factor (Qin et al., 2017).

3. Results and discussion

3.1. Field evidence show strong coupling of P and Mn

DGT-P and DGT-Mn in sediment profiles showed synchronously distributed and significantly positive correlated (Winter: $r^2 > 0.37$, $p < 0.01$; Spring: $r^2 > 0.21$, $p < 0.05$; summer: $r^2 > 0.40$, $p < 0.01$; autumn: $r^2 > 0.64$, $p < 0.01$) (Fig. 1 and S6), suggests the close association of P cycle with Mn. Besides, higher concentration of DGT-P and DGT-Mn near the SWI in summer and autumn compared with that in winter and spring, suggests higher release fluxes of P and Mn both in in the Summer and Autumn. In contrast, random distributions and poor or negative correlations between DGT-P and DGT-Fe from the one-year

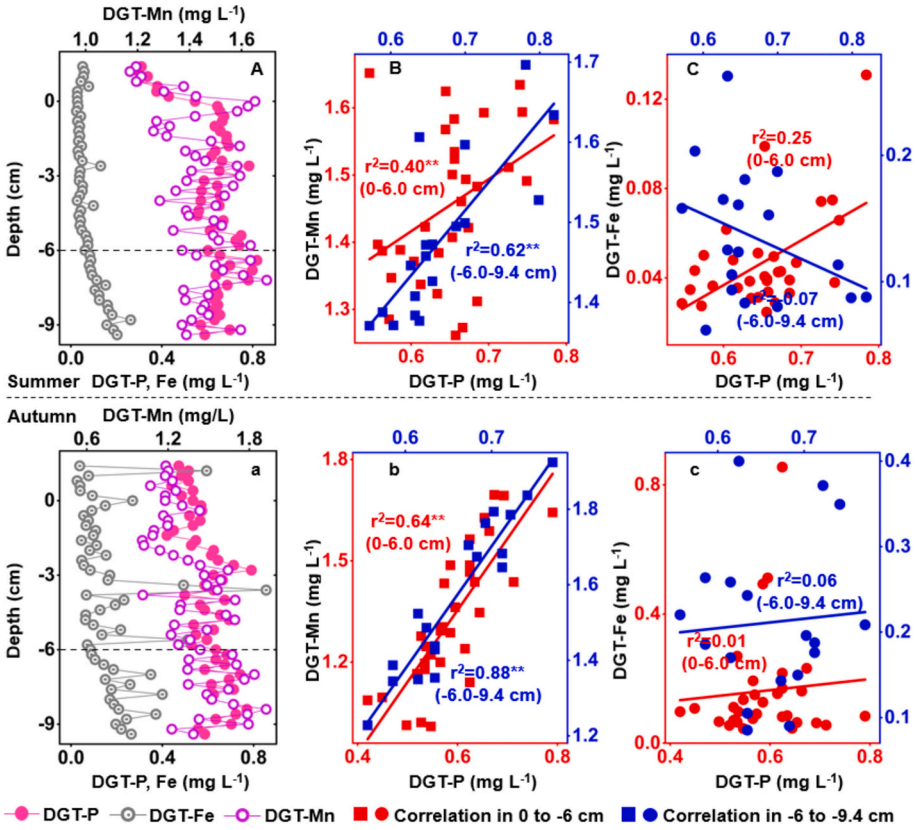

Fig. 1. Sediment depth profiles and correlation analyses of DGT—P, —Fe, and —Mn concentrations in field investigations. (A) Sediment depth profile of DGT—P, —Fe, and —Mn concentrations in Summer. (B) Correlation analyses between DGT-P and DGT-Mn concentrations in Summer, Red and blue symbols represent correlation analyses at the depth of 0 to −6 cm and − 6 to −9.4 cm, respectively. (C) Correlation analyses between DGT-P and DGT-Fe concentrations in Summer, Red and blue symbols represent correlation analyses at the depth of 0 to −6 cm and − 6 to −9.4 cm, respectively. Autumn investigations were presented correspondingly in a, b, and c. The sediment-water interfaces were set at the depth of 0 cm.

field monitoring indicated a negligible influence of Fe on P mobilization (Fig. 1 and S6). These observations were not consistent with the previous findings that Fe controlled P cycling in aquatic ecosystems (Mortimer, 1941; Rydin, 2000; Smith et al., 2011; Ding et al., 2016a). Consistently with our results, some studies also documented the coupled geochemical behavior of P and Mn in sediments (Schroth et al., 2015; Hermans et al., 2019; Pan et al., 2019; Li et al., 2021; Zhou et al., 2024), indicating the coupled cycling between P and Mn were existed in aquatic sediments. Herein, we observed the coupled mobilization of P and Mn during anoxic period (O_2 concentrations <2 mg L^{-1}, Fig. S3) in the yearlong field investigation, further confirming the important role of Mn in controlling P mobilization.

Surprisingly, the coupled cycling of P with Mn observed in Aha reservoir was totally different with our previous observation in Hongfeng reservoir (Chen et al., 2019b), despite a mere 23 km physical distance between them. The reducing sedimentary conditions in Aha reservoir is likely to cause Fe/Mn deposited in a more reduced state (Kang et al., 2018), providing an opportunity for Mn to drive P mobilization (Chen et al., 2018; Chen et al., 2019b). Taken together, this is an in-situ high-resolution field investigation reported the couple cycling of P and Mn in reservoir sediments. More evidence to support this argument will be shown below.

3.2. Laboratory evidence confirm strong coupling of P and Mn

To further investigate the geochemical behaviors of P and Mn, laboratory incubation experiments were conducted using four sediment cores collected from Aha reservoir's dam site (Fig. S5). For the cores were incubated under oxic conditions, the synchronized distributions and significant positive correlation ($r^2 > 0.64$, $p < 0.01$) between DGT-Mn and DGT-P further confirmed the strong association of P with Mn (Fig. S7A—B). The lower mean concentrations of DGT-P (0.18 mg L^{-1}) and DGT-Mn (0.14 mg L^{-1}) in the overlying water suggested that P and Mn were less diffused back into overlying water. This is likely attributed to Mn^{2+} and Fe^{2+} were oxidized to form amorphous Mn/Fe(*oxy*)hydroxides when encountered O_2 among the top few millimeters of the sediment (Davison, 1993). Then P was trapped by these Mn/Fe(*oxy*) hydroxides. Meanwhile, poor correlations ($r^2 < 0.13$) between DGT-P and DGT-Fe indicated the negligible role of Fe on P cycle (Fig. S7C). The peak concentration of DGT-Fe near the SWI is likely because O_2 promotes the local degradation of organic matter that induces intensive Fe mobilization (Davison, 1993; Zhou et al., 2020). The low concentration of DGT-Fe at the depths of 0 to −6 cm is likely because Fe^{2+} was trapped by sulfide then deposited in sediments (Fig. S8).

For the cores were incubated under anoxic conditions, P also showed strong correlation with Mn ($r^2 > 0.63$, $p < 0.01$) and the poor correlation ($r^2 < 0.35$) with Fe further confirming the couple cycling of P and Mn in sediments (Fig. S7b-c). The higher mean concentrations of DGT-P (0.68 mg L^{-1}) and DGT-Mn (0.64 mg L^{-1}) in overlying water, which are 3.8- and 4.6-folds higher than those under oxic conditions, demonstrating a stronger degree of the co-released of P and Mn from sediments. This is likely due to the disappearance of the oxic/anoxic boundary at the SWI allowed Mn, P and Fe could diffuse freely into the overlying water (Fig. S7a) (Schroth et al., 2015).

Concurrent accumulations of P and Mn were observed in the overlying water form anoxic incubated cores, further demonstrating the co-released of P and Mn from the sediments (Fig. 2A-B). The concentrations of TP, SRP, Mn, and Fe at the beginning (day-1) of incubation

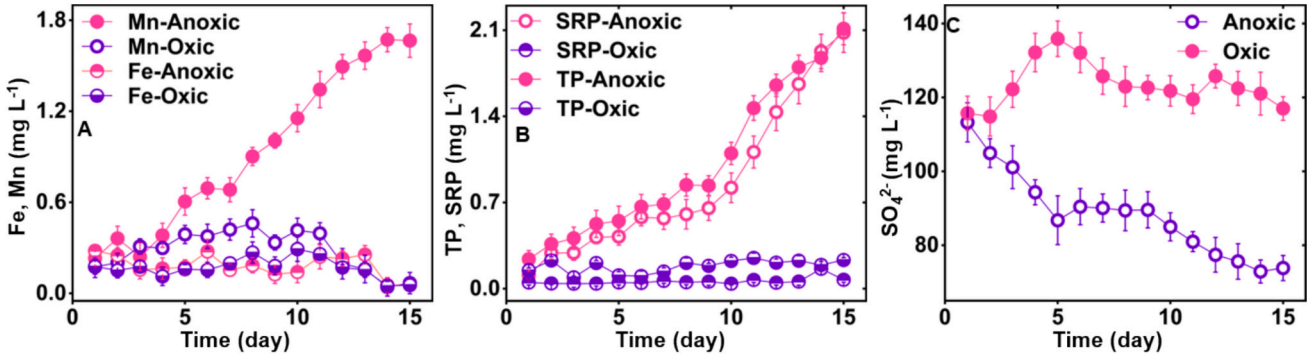

Fig. 2. Variations of daily overlying water of Fe, Mn, P, and SO_4^{2-} concentrations in laboratory incubation experiments. (A) Mn and Fe concentrations, (B) total phosphorus (TP) and soluble reactive phosphorus (SRP) concentrations, and (C) sulfate (SO_4^{2-}) concentrations.

experiments were 0.24, 0.11, 0.23, and 0.28 mg L^{-1}, respectively (Fig. 2A-B). To the end of the incubation experiments (day-15), the concentrations of TP, SRP, and Mn reached at 2.11, 2.08, and 1.76 mg L^{-1}, respectively. However, the concentration of Fe also remained at a steady low level (mean: 0.18 mg L^{-1}). This is likely because Fe^{2+} was coprecipitated with sulfide to form FeS in sediments (Fig. S8), as the sulfate concentration under anoxic condition was continuously decreased (Fig. 2C). Furthermore, a significant positive correlation ($r^2 = 0.96$, $p < 0.01$) between net increase P and Mn concentrations were observed in the overlying water from the cores incubated under anoxic, indicated that the release of P was strong associated with Mn from the sediments. In the overlying water from the cores incubated under oxic, the concentrations of Mn, Fe, TP, SRP, and sulfate maintained in a steady low state, implied that there was less net release from sediments (Fig. 2). These results collectively suggest that Mn and P were continuously released from the sediment in a synchronized manner and accumulated in the overlying water.

Besides, the simultaneous release of P and Mn was also observed from solid sediment fractions (Fig. S9). Under anoxic conditions, the mean contents of NH_4Cl-P, acid extracted-Mn, and acid extracted-Fe were 5.3, 64.3, and 22.8 mg kg^{-1}, respectively, accounting for only 62.4 %, 48.7 %, and 49.4 % of those under oxic conditions (NH_4Cl-P: 8.5 mg kg^{-1}, acid extracted-Mn: 132.1 mg kg^{-1}, and acid extracted-Fe: 46.2 mg kg^{-1}). Results showed that 37.6 % of NH_4Cl-P, 51.3 % of acid extracted-Mn, and 50.6 % of acid extracted-Fe would be released when the environmental conditions shifted from oxic to anoxic. It was worth noting that although the mean contents of total Fe were 4.7-times higher than that of total Mn (Fe: 53.0 g kg^{-1}, Mn: 11.4 g kg^{-1}) in sediments, mean acid extracted-Mn contents (98.2 mg kg^{-1}) was 2.6-times higher than that of mean acid extracted-Fe (34.5 mg kg^{-1}). This was likely because Fe^{2+} could be easily trapped by sulfide to form FeS which is considerably more insoluble than MnS [$K_{sp}(FeS) = 6.3 \times 10^{-18}$, $K_{sp}(MnS) = 2.5 \times 10^{-13}$] (Davison, 1993). In contrast, Mn^{2+} could be overturned more freely to generate amorphous Mn(*oxy*)hydroxide (Acid Ex-Mn) under oxic environment and reduced under anoxic environment (Madison et al., 2013). Moreover, a more significant positive correlation between net NH_4Cl-P and net acid extracted-Mn concentrations at the top 7 cm sediment, suggesting that P is simultaneous released with Mn and not with Fe (Table S2).

3.3. Microscopic mechanisms of Mn driving P mobilization

3.3.1. Mn is more likely to drive P mobilization than Fe thermodynamically

Recognition for the thermodynamic processes of Mn/Fe are useful for understanding the mechanism of Fe/Mn redox on driving P mobilization. Generally, the redox reaction of Mn/Fe can be formulated as the sum of two half-reactions with the oxidation of reductants and the reduction of oxidants from different redox couples (Luther, 2009; Borch et al., 2010). Besides, both O_2 and NO_3^- have been demonstrated as the most prevalence oxidants in most aquatic ecosystems, and the oxidation rate of Mn^{2+}/Fe^{2+} have been evidenced to be controlled by the first accepted electron of O_2 and NO_3^- (Luther, 2005, 2009; Colombo et al., 2023). Theoretically, the oxidation of Mn^{2+} is thermodynamically unfavorable while that of Fe^{2+} is thermodynamically favorable based on the thermodynamic calculations using Gibbs free energies of coupling half reactions in the pH range from 1 to 13 (Fig. 3). Those results implied that the reduction of Mn oxides is thermodynamically favorable while that of Fe oxides are thermodynamically unfavorable.

Theoretically, depending on the Fe oxides formed, the one-electron oxidation of Fe^{2+} by O_2 could occur in a low pH at 5.2 (Fig. 3A, the detail of thermodynamic calculations was presented in Text S2). However, the oxidation of Mn^{2+} by O_2 only occur in a high pH ranging from pH 8.4 to 11.8. Similarly, when the oxidant is NO_3^-, the oxidation of Fe^{2+} could theoretically occur at a lower pH (2.6) or even without pH limit. In contrast, the oxidation of Mn^{2+} cannot occur or only occur within a remarkable high pH range from 8.9 to 12.3, whereas those high pH conditions are less or lack existed in nature aquatic environmental (Fig. 3B). Those above theoretical calculations indicated that Fe oxidation is easy occurred and fast, versus Mn oxidation is difficult and slow. For the reduction, it was obvious that the reduction of Mn would be priority and ease compare with that of Fe, which could lead to the redox of Mn is more likely to drive P mobilization.

3.3.2. Mn(III) is the key species to dominate the mobilization of P

The mechanism of P mobilization driven by Mn redox, evidenced by XPS, suggests that P is likely complexed with Mn oxides to form P-bearing Mn complexes then deposited on the sediment pellets surface under oxic conditions; Subsequently, those P-bearing Mn complexes were reduced under anoxic conditions leading to the simultaneous release of Mn and P (Fig. 4). For the top 1 cm sediment pellets under anoxic conditions, the contents of P (35.4 mM) and Mn (183.7 mM) in outer layer were lower than that in inner layer (P:37.5 mM; Mn:185.5 mM) (Fig. 4A and C, Table S3). In contrast, under oxic conditions, the spectra intensity of P (contents: 42.5 mM) and Mn (contents: 210.3 mM) in outer layer have increased much stronger than that in inner layer (Fig. 4a and c, Table S3). Notably, atomic amount of P and Mn under oxic conditions increased by 20.0 % and 14.5 % compared to that under anoxic conditions (Table S3). Those results collectively evidenced that P and Mn were re-enriched synchronously in sediment pellet surface when the environment condition shifted from anoxic to oxic. Meanwhile, the spectra intensity of P and Mn both in out and inner layer at the depth of 9 cm were weak with an atomic ratio of P: Mn: Fe showed minor fluctuations around 1.08: 6.11: 29.63 (Fig. 4B-b and D-d, Table S3), implied that the contents of P and Mn in deep sediments changed less. Besides, the spectra intensity of Fe in pellet outer layer were always weaker than that in inner layer (Fig. S10A-a and S10B-b), evidenced that Fe was mainly deposited in pellet inner layer and Fe was little cycled when environmental conditions change.

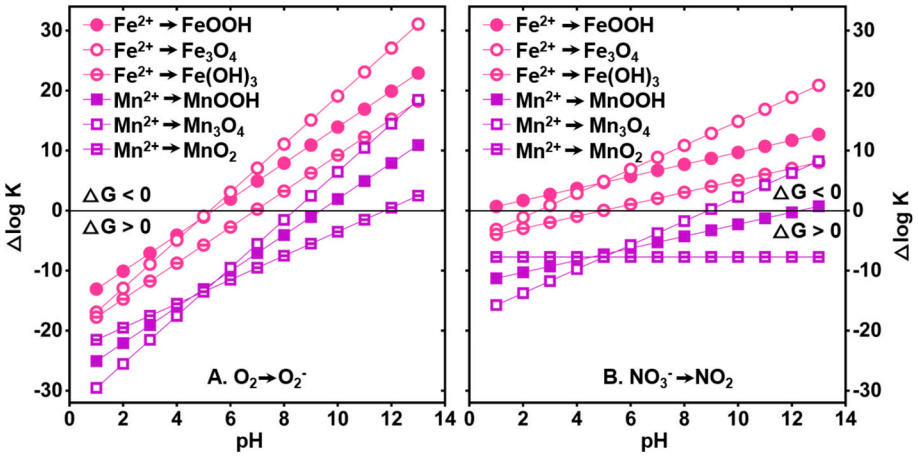

Fig. 3. One-electron transfer reactions of Fe^{2+} and Mn^{2+} with the first electron accepted by (A) O_2 to form O_2^-, and (B) NO_3^- to form NO_2. The +△log K on the y-axis indicates a favorable complete reaction and -△log K indicates an unfavorable reaction as $\triangle G^o = -RT\ lnK = -2.303\ RT\ log\ K$, thermodynamic calculation data were taken from Luther (2009). The detail of thermodynamic calculation was shown in Text S2.

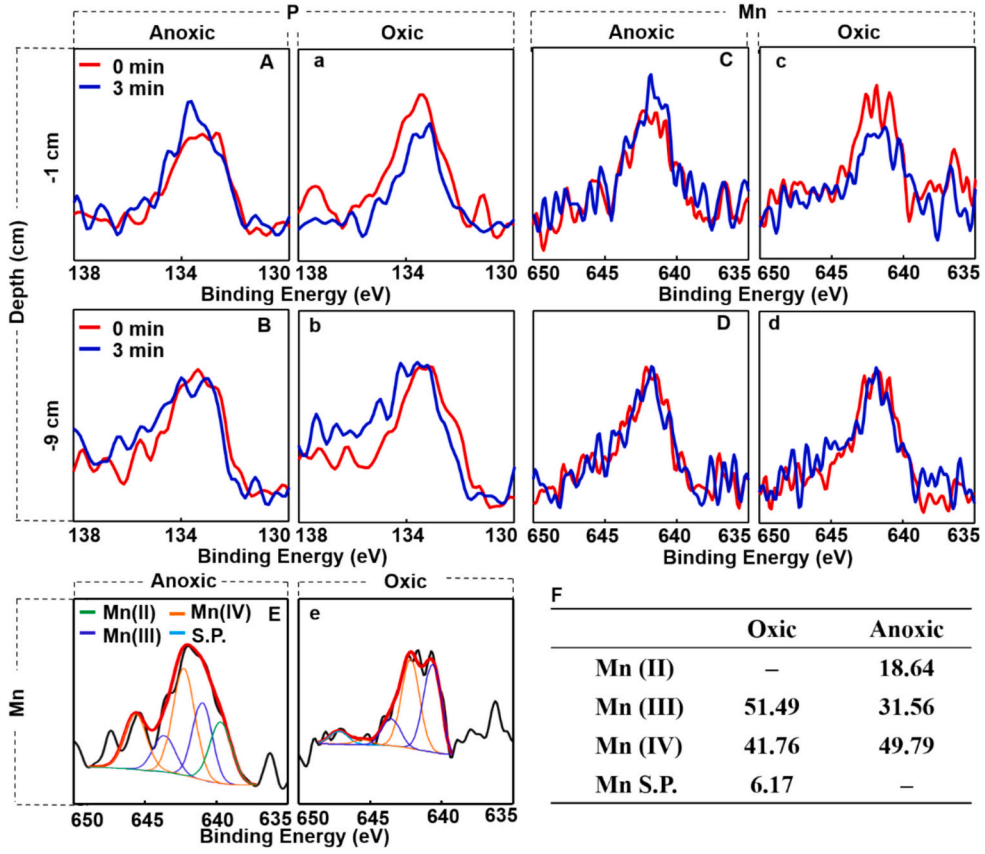

F

	Oxic	Anoxic
Mn (II)	–	18.64
Mn (III)	51.49	31.56
Mn (IV)	41.76	49.79
Mn S.P.	6.17	–

Fig. 4. XPS spectra analysis of P and Mn in sediment pellet depth profile of laboratory incubation experiments. Spectra were collected at the XPS probing time of 0 and 3 min and their corresponding depth is 0–3 and 3–17 nm, respectively. A and B are the XPS spectra of P under anoxic conditions at the depth of −1 and − 9 cm, respectively. P spectra under oxic conditions were presented in a and b. C and D are the XPS spectra of Mn under anoxic conditions at the depth of −1 and − 9 cm, respectively. Mn spectra under oxic conditions were presented in c and d. E and e are Mn valence fitting based on XPS spectral from the outer layer (0–3 nm) at the uppermost 1 cm sediment, the corresponding fitting results were presented in Table F. "S.P." is the abbreviation of satellite peaks. "–" indicates that the content is below the detection limit of the instrument.

Specifically, XPS valence results further revealed that P mobilization was mainly associated with Mn^{3+} cycle (Fig. 4E-e and F). Compared with Mn^{4+}, Mn^{3+} has stronger adsorption for phosphate as its higher ionic potential (Madison et al., 2013; Wang et al., 2024). Under anoxic conditions, the contents proportion of Mn^{2+} in sediment pellet surface was 18.64 %, while that was below the detection limit of instrument under oxic conditions (Fig. 4F). This suggested that Mn^{2+} was oxidized totally when redox conditions changed from anoxic to oxic. Notably, the proportion of Mn^{3+} contents in Mn pools were 51.49 % under oxic conditions, which was around 20 % higher than that under anoxic conditions (31.56 %). Besides, the proportion of Mn^{4+} content was reduced by about 8 % under oxic conditions compared to anoxic

conditions. Those results indicated that Mn^{3+} has intensive geochemical cycle when the condition changed. Similar results were observed from Mn K-edge XANES analyses (Fig. S11). For the sediment sample at the top 1 cm under anoxic conditions, Mn^{2+} (i.e $MnCO_3$,) contents from outer layer (0–3 nm) in sediments pellets own around 10 % proportion in Mn pools. Whereas Mn^{2+} contents were below the detection limit of instrument under oxic conditions (Fig. S11A-a). Obviously, the XANES results also presented similar geochemical behavior that Mn^{2+} was oxidized completely when the environmental conditions changed from anoxic to oxic.

Obviously, redox of Mn^{4+} may also affect the mobilization of P in sediments. Mn^{4+} has poor adsorption capacity to phosphate and organic matter when it was existed alone (Simanova et al., 2015). However, the presence of Ca^{2+} and Mg^{2+} would favor the adsorption of OMs such as fulvic acid by Mn^{4+} to form Mn^{4+}-OM complexes under weakly alkaline conditions (Zhu et al., 2010; Wang et al., 2019a; Wang et al., 2024), those Mn^{4+}-OM complexes were expected to be an effective scavenger to phosphate (Davison, 1993; Madison et al., 2013). Herein, the mean proportion of Mn^{4+} contents in Mn pools were >44.5 % (Fig. 4F and S11A-a), this indicated that there are abundant Mn^{4+} oxides in sediments. Meanwhile, sediments porewater of Aha Reservoir showed weak alkalinity (pH:7.3), and the mean concentrations of Ca^{2+} and Mg^{2+} were 2.75 and 0.88 mM, respectively (Table S4). Besides, XPS spectra intensity of carbon in pellets outer layer was strong along sediment profile indicated that there are abundant OMs in this system (Fig. S10C-c and S10D-d). Those high concentration of divalent cations and OMs can favor Mn^{4+} adsorb phosphate under oxic conditions, then the reduction of OM-Mn-P complexes could contribute for P mobilization under anoxic conditions.

Most importantly, DB-SEM images, at the top 1 cm of sediment samples from both indoor oxic incubations and field-collected sediment cores, showed Mn and P are strongly co-enriched in the same zone (Fig. 5 and S12). Although Fe was also enriched in the same zone, combined with above determined results: 1) P and Mn were synchronously re-enriched in sediment pellet surface when the environment condition shifted from anoxic to oxic (Fig. 4A-a and 4C-c); 2) DGT-P and DGT-Mn showed synchronously distributed and significantly positive correlated both from field investigation and laboratory incubated experiments (Fig. 1 and S7); and 3) P and Mn were simultaneous release from sediment and accumulated in anoxic overlying water (Fig. 2 and S9). Those results collectively confirmed that P was mainly hosted by Mn oxides and P mobilization was controlled by the redox of Mn not by Fe.

3.3.3. *Decoupling of P and Fe in reducing sediments*

Fe is mainly deposited as inert Fe minerals that are weakly adsorbed/complexed with P, this is responsible for the decoupling of P and Fe in reducing sediments. The general low mean concentration of DGT-Fe (0.18 mg L^{-1}) were observed at the top 6 cm sediment in both field investigation and incubation experiments (Fig. 1 and S7). This may be attributed to the fact that Fe(II) was trapped by abundant S(-II) (>0.45 mg L^{-1}) (Fig. S8), resulting in Fe mainly deposited as inert Fe minerals. Because the continuously decreased sulphate concentrations in the overlying water from the anoxic incubated cores indicated that strong reduction of sulphate did occur (Fig. 2C and S8). Above perspectives were further evidenced by the results that proportion of inert Fe minerals is over 99.2 % in Fe pools from chemical sequential extraction (Resid-Fe; Fig. S9C-c).

Consistently, both results from Fe K-edge XANES (Pyrite+Ferri+$FeSO_4$) and Mössbauer spectroscopy (Pyrite+$FeSO_4$) showed that the proportion of reduced Fe (Fe^{2+}) in Fe pools is generally above 41 % (Fig. S11B-b and S13). Those results evidenced the ratio of Fe^{3+}/Fe^{2+} was <1.5, which further demonstrating that this is a reducing sedimentary environment (Kang et al., 2018). Notably, it was unconvinced to conclude that P was decoupled with Fe solely based on the poor correlations between DGT-P and DGT-Fe at the top 6 cm sediments, due to Fe(II) maybe being trapped rapidly by S(-II) during Fe and P simultaneously released (Fig. 1 and S7). In the depth range from −6 to −9.4 cm, DGT-Fe concentration gradually increased and the DGT-S concentration decreased (Fig. S8). This may be mainly because the fact that only a small amount of Fe(II) was captured by S(-II), as the metabolism of sulfate-reducing bacteria was weakened among this depth range (Rozan et al., 2002; Pan et al., 2023). However, DGT-P was also poor correlated with DGT-Fe and significantly correlated with DGT-

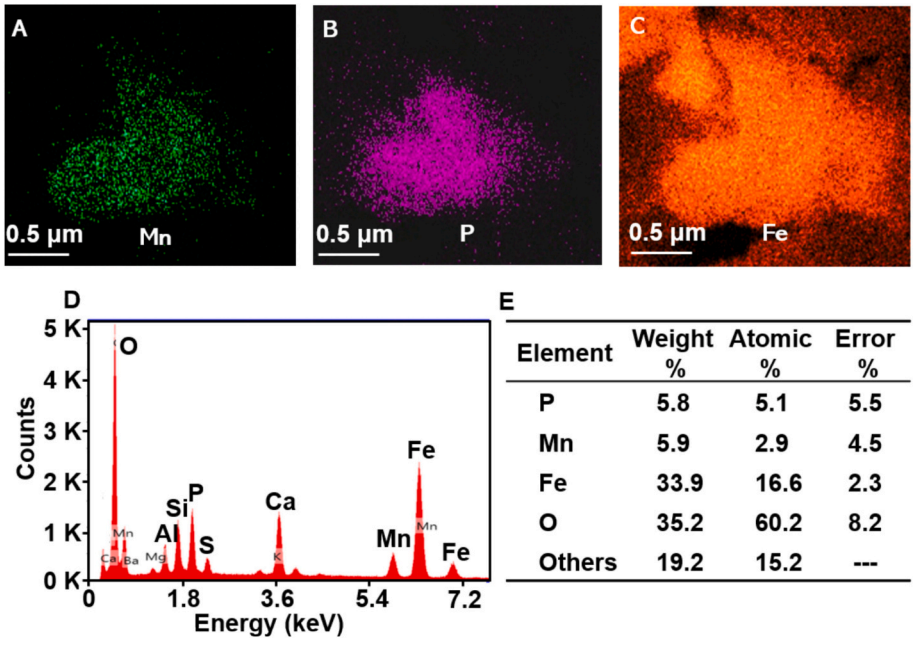

E

Element	Weight %	Atomic %	Error %
P	5.8	5.1	5.5
Mn	5.9	2.9	4.5
Fe	33.9	16.6	2.3
O	35.2	60.2	8.2
Others	19.2	15.2	---

Fig. 5. Two-dimensions, high-resolution SEM maps of Mn (green), P (violet), and Fe (red) of the top 1 cm sediments sample from the cores incubated under oxic conditions. These maps are shown in true zone and the brightness was adjusted to emphasize the distributions of Mn, P, and Fe in the sediments. (A) distribution of Mn, (B) distribution of P, and (C) distribution of Fe, (D) SEM-EDS analysis of sediment samples, (E) contents of P, Mn, and Fe in the sediment.

Mn (Fig. 1 and S7), further confirmed that P was mainly bound with Mn not with Fe. Those results collectively offered convince evidences for the weak influence of Fe on P mobilization.

3.3.4. Advance understanding for the mobilization of P in aquatic sediments

Generally, we summarized and proposed the mechanisms of P mobilization in different sedimentary environments based on above discussion. In oxidizing sediments ($Fe^{3+}/Fe^{2+} > 3.0$) with abundant amorphous Fe (oxy)hydroxides (Kang et al., 2018), intense biogeochemical processes occurred frequently, which likely existed in new to middle-aged reservoirs with abundant organic matters (Chen et al., 2018, 2023). The redox of Fe usually dominates the mobilization of P (Ding et al., 2016a; Chen et al., 2019b; Xiong et al., 2023), the weak effect of Mn on P mobilization is difficult to detect then is often overlooked (Chen et al., 2019a). This is a classical mechanism of P mobilization which scientists have long recognized. In contrast, in reducing sediments which have already undergone intense biogeochemical processes, due to most of Fe had deposited as inert Fe minerals (Fig. S8 and S9), the effect of Fe on P mobilization would be hidden and the mobilization of P is more inclined to be driven by Mn redox. Consistently, our theoretical calculations support this view that Mn (oxy)hydroxides are more readily reduced than Fe (oxy)hydroxides (Fig. 3). As such, the reduction of Mn will preferentially dominate P mobilization in reducing sediments. Taken together, this study reports advance understanding for the mobilization of P in reducing sediments, and reveals the underlying mechanism of P mobilization was mainly driven by the redox of Mn^{3+}.

4. Conclusion

This study provides a new insight into P cycle and offers clear evidence that P mobilization is primarily driven by Mn(III) in reducing sediments. Despite Fe inevitably interferes with P cycling, both results from field and laboratory incubations clearly evidenced synchronized distributions and significant positive correlations between P and Mn, which in turn confirms the priority control of Mn for P cycling. Moreover, we evidenced that P was complexed with Mn oxides to form P-bearing Mn complexes then deposited in sediment pellet surface under oxic conditions, then the rapid reduction of Mn oxides lead to the simultaneous release of P and Mn when environmental conditions shifted into anoxic. The Mn(III) was evidenced to be the key specie to dominate P mobilization in reducing sediments. Fe mainly deposited as inert Fe minerals, which responsible for the decouple between P cycle and Fe in reducing sediment. Finally, an updated P cycling patterns in different sedimentary environments were proposed with P mobilization was controlled by Fe in oxidizing sedimentary environments while that was driven by Mn in reducing sedimentary environments. Taken together, the mobilization of P driven by Mn in reducing sediments observed in this study may help to understand the influence of Mn even other non-Fe metals on the P cycle in aquatic ecosystems, further advancing the remediation and management of eutrophication. Particularly, the intensive release of P from sediments caused by stratification is becoming prevalent in most aging reservoirs.

CRediT authorship contribution statement

Quan Chen: Writing – original draft, Methodology, Investigation, Formal analysis, Data curation. **Jing-fu Wang:** Writing – review & editing, Validation, Supervision, Conceptualization. **Meng-qiang Zhu:** Writing – review & editing. **Hai-bo Qin:** Data curation. **Peng Liao:** Writing – review & editing, Methodology. **Zhi-tong Lu:** Investigation, Data curation. **Peng-cheng Ju:** Writing – review & editing. **Jing-an Chen:** Writing – review & editing, Project administration, Funding acquisition, Conceptualization.

Declaration of competing interest

The authors declare that they have no known competing financial interests or personal relationships that could have appeared to influence the work reported in this paper.

Data availability

Data will be made available on request.

Acknowledgments

This study was sponsored jointly by the National Key Research and Development Plan of China (No. 2023YFF0806000 and 2021YFC3201000), the Strategic Priority Research Program of CAS (No. XDB40020400), the Postdoctoral Fellowship Program of CPSF under Grant Number GZC20241694, the Chinese NSF project (No. 41977296, 42277253), the Guizhou Provincial Science and Technology Program (Qiankehe Platform Talents-YQK[2023]034, Qiankehe Platform-YWZ [2023]006), and the Outstanding member of Youth Innovation Promotion Association CAS (Y2023105).

Appendix A. Supplementary data

Supplementary data to this article can be found online at https://doi.org/10.1016/j.scitotenv.2024.176564.

References

Alcott, L.J., Mills, B.J.W., Poulton, S.W., 2019. Stepwise earth oxygenation is an inherent property of global biogeochemical cycling. Science 366 (6471), 1333–1337.
Bjerrum, C.J., Canfield, D.E., 2002. Ocean productivity before about 1.9 Gyr ago limited by phosphorus adsorption onto iron oxides. Nature 417 (6885), 159–162.
Borch, T., Kretzschmar, R., Kappler, A., Van Cappellen, P., Ginder-Vogel, M., Voegelin, A., Campbell, K., 2010. Biogeochemical redox processes and their impact on contaminant dynamics. Environ. Sci. Technol. 44 (1), 15–23.
Chen, J.A., Wang, J.F., Guo, J.Y., Yu, J., Zeng, Y., Yang, H.Q., Zhang, R.Y., 2018. Eco-environment of reservoirs in China. Prog. Phys. Geogr. 42 (2), 185–201.
Chen, M., Ding, S., Wu, Y., Fan, X., Jin, Z., Tsang, D.C.W., Wang, Y., Zhang, C., 2019a. Phosphorus mobilization in lake sediments: experimental evidence of strong control by iron and negligible influences of manganese redox reactions. Environ. Pollut. 246, 472–481.
Chen, Q., Chen, J.A., Wang, J.F., Guo, J.Y., Jin, Z.X., Yu, P.P., Ma, Z.Z., 2019b. In situ, high-resolution evidence of phosphorus release from sediments controlled by the reductive dissolution of iron-bound phosphorus in a deep reservoir, southwestern China. Sci. Total Environ. 666, 39–45.
Chen, Q., Xu, S., Wang, J., Wang, D., Dai, Z., Liao, P., Yang, J., Guo, W., Ding, S., Chen, J., 2023. Application of two-dimension, high-resolution evidences to reveal the biogeochemical process patterns of trace metals in reservoir sediments. Sci. Total Environ. 900, 166404.
Colombo, M., LaRoche, J., Desai, D., Li, J.X., Maldonado, M.T., 2023. Control of particulate manganese (Mn) cycling in halocline Arctic Ocean waters by putative Mn-oxidizing bacterial dynamics. Limnol. Oceanogr. 68, 2070–2087.
Conley, D.J., Paerl, H.W., Howarth, R.W., Boesch, D.F., Seitzinger, S.P., Havens, K.E., Lancelot, C., Likens, G.E., 2009. ECOLOGY: controlling eutrophication: nitrogen and phosphorus. Science 323 (5917), 1014–1015.
Dadi, T., Schultze, M., Kong, X.Z., Seewald, M., Rinke, K., Friese, K., 2023. Sudden eutrophication of an aluminum sulphate treated lake due to abrupt increase of internal phosphorus loading after three decades of mesotrophy. Water Res. 235, 119824.
Davison, W., 1993. Iron and manganese in lakes. Earth Sci. Rev. 34, 119–163.
Davison, W., Zhang, H., 1994. In situ speciation measurements of trace components in natural waters using thin-film gels. Nature 367 (6463), 546–548.
Ding, S., Xu, D., Sun, Q., Yin, H., Zhang, C., 2010. Measurement of dissolved reactive phosphorus using the diffusive gradients in thin films technique with a high-capacity binding phase. Environ. Sci. Technol. 44, 8169–8174.
Ding, S.M., Sun, Q., Xu, D., Jia, F., He, X., Zhang, C.S., 2012. High-resolution simultaneous measurements of dissolved reactive phosphorus and dissolved sulfide: the first observation of their simultaneous release in sediments. Environ. Sci. Technol. 46 (15), 8297–8304.

Ding, S.M., Wang, Y., Wang, D., Li, Y.Y., Gong, M., Zhang, C.S., 2016a. In situ, high-resolution evidence for iron-coupled mobilization of phosphorus in sediments. Sci. Rep. 6, 24341.
Ding, S.M., Wang, Y., Zhang, L., Xu, L., Gong, M., Zhang, C.S., 2016b. New holder configurations for use in the diffusive gradients in thin films (DGT) technique. RSC Adv. 6 (91), 88143–88156.
Dodd, M.S., Shi, W., Li, C., Zhang, Z., Cheng, M., Gu, H., Hardisty, D.S., Loyd, S.J., Wallace .vS., M.W., Hood, A., Lamothe, K., Mills, B.J.W., Poulton, S.W., Lyons, T.W., 2023. Uncovering the Ediacaran phosphorus cycle. Nature 618, 974–980.
Duhamel, S., Diaz, J.M., Adams, J.C., Djaoudi, K., Steck, V., Waggoner, E.M., 2021. Phosphorus as an integral component of global marine biogeochemistry. Nat. Geosci. 14, 359–368.
Hermans, M., Lenstra, W.K., van Helmond, N.A.G.M., Behrends, T., Egger, M., Séguret, M.J.M., Gustafsson, E., Gustafsson, B.G., Slomp, C.P., 2019. Impact of natural re-oxygenation on the sediment dynamics of manganese, iron and phosphorus in a euxinic Baltic Sea basin. Geochim. Cosmochim. Acta 246, 174–196.
Hupfer, M., Gachter, R., Giovanoli, R., 1995. Transformation of phosphorus species in settling seston and during early sediment diagenesis. Aquat. Sci. 57 (4), 305–324.
Ingall, E., Jahnke, R., 1994. Evidence for enhanced phosphorus regeneration from marine sediments overlain by oxygen depleted waters. Geochim. Cosmochim. Acta 58 (11), 2571–2575.
Ji, N., Liu, Y., Wang, S., Wu, Z., Li, H., 2022. Buffering effect of suspended particulate matter on phosphorus cycling during transport from rivers to lakes. Water Res. 216, 118350.
Jones, C., Nomosatryo, S., Crowe, S.A., Bjerrum, C.J., Canfield, D.E., 2015. Iron oxides, divalent cations, silica, and the early earth phosphorus crisis. Geology 43 (2), 135–138.
Kang, T., Song, L., Zheng, X., Huang, Y., Yang, J., Teng, Y., 2018. Iron and manganese cycling and vertical distribution of heavy metals in sediments of Aha Lake and Hongfeng Lake. Chinese J. Ecol. 37 (3), 751–762.
Kipp, M.A., Stüeken, E.E., 2017. Biomass recycling and Earth's early phosphorus cycle. Sci. Adv. 3 (11), eaao4795.
Konhauser, K.O., Amskold, L., Lalonde, S.V., Posth, N.R., Kappler, A., Anbar, A., 2007a. Decoupling photochemical Fe(II) oxidation from shallow-water BIF deposition. Earth Planet. Sc. Lett. 258 (1–2), 87–100.
Konhauser, K.O., Lalonde, S.V., Amskold, L., Holland, H.D., 2007b. Was there really an Archean phosphate crisis? Science 315 (5816), 1234.
Li, R., Gao, L., Wu, Q.R., Liang, Z.B., Hou, L., Yang, Z.G., Chen, J.Y., Jiang, T., Zhu, A.P., Li, M.Z., 2021. Release characteristics and mechanisms of sediment phosphorus in contaminated and uncontaminated rivers: a case study in South China. Environ. Pollut. 268, 115749.
Luther, G.W., 2005. Manganese(II) oxidation and Mn(IV) reduction in the environment-two one-Electron transfer steps versus a single two-Electron step. Geomicrobiol J. 22 (3–4), 195–203.
Luther, G.W., 2009. The role of one- and two-Electron transfer reactions in forming thermodynamically unstable intermediates as barriers in multi-Electron redox reactions. Aquat. Geochem. 16 (3), 395–420.
Ma, S., Banfield, J.F., 2011. Micron-scale Fe^{2+}/Fe^{3+}, intermediate sulfur species and O_2 gradients across the biofilm–solution–sediment interface control biofilm organization. Geochim. Cosmochim. Acta 75 (12), 3568–3580.
Maavara, T., Chen, Q., Van Meter, K., Brown, L.E., Zhang, J., Ni, J., Zarfl, C., 2020. River dam impacts on biogeochemical cycling. Nat. Rev. Earth & Env. 1 (2), 103–116.
Maavara, T., Parsons, C.T., Ridenour, C., Stojanovic, S., Durr, H.H., Powley, H.R., Van Cappellen, P., 2015. Global phosphorus retention by river damming. Proc. Nati. Acad. Sci. U. S. A. 112 (51), 15603–15608.
Madison, A.S., Tebo, B.M., Mucci, A., Sundby, B., Luther, G.W., 2013. Abundant porewater Mn(III) is a major component of the sedimentary redox system. Science 341 (6148), 875–878.
Maure, E.R., Terauchi, G., Ishizaka, J., Clinton, N., DeWitt, M., 2021. Globally consistent assessment of coastal eutrophication. Nat. Commun. 12 (1), 6142.
Ming, C.L., Breef-Pilz, A., Howard, D.W., Schreiber, M.E., 2024. Geochemical drivers of manganese removal in drinking water reservoirs under hypolimnetic oxygenation. Appl. Geochem. 172, 106120.
Mortimer, C.H., 1941. The exchange of dissolved substances between mud and water in lakes. J. Ecol. 29 (2), 280–329.
Murphy, J., Riley, J.P., 1962. A modified single solution method for the determination of phosphate in natural waters. Anal. Chim. Acta 27, 31–36.
Nemati, K., Abu Bakar, N.K., Abas, M.R., Sobhanzadeh, E., 2011. Speciation of heavy metals by modified BCR sequential extraction procedure in different depths of sediments from Sungai Buloh, Selangor. Malaysia. J. Hazard. Mater. 192 (1), 402–410.
Pan, F., Liu, H., Guo, Z., Cai, Y., Fu, Y., Wu, J., Wang, B., Gao, A., 2019. Metal/metalloid and phosphorus characteristics in porewater associated with manganese geochemistry: a case study in the Jiulong River estuary. China. Environ. Pollut. 255 (1), 113134.
Pan, F., Xiao, K., Cai, Y., Li, H., Guo, Z., Wang, X., Zheng, Y., Zheng, C., Bostick, B.C., Michael, H.A., 2023. Integrated effects of bioturbation, warming and sea-level rise on mobility of sulfide and metalloids in sediment porewater of mangrove wetlands. Water Res. 233, 119788.
Paytan, A., McLaughlin, K., 2007. The oceanic phosphorus cycle. Chem. Rev. 107 (2), 563–576.
Poulton, S.W., 2003. Sulfide oxidation and iron dissolution kinetics during the reaction of dissolved sulfide with ferrihydrite. Chem. Geol. 202 (1), 79–94.
Poulton, S.W., Krom, M.D., Raiswell, R., 2004. A revised scheme for the reactivity of iron (oxyhydr)oxide minerals towards dissolved sulfide. Geochim. Cosmochim. Acta 68 (18), 3703–3715.
Powers, S.M., Bruulsema, T.W., Burt, T.P., Chan, N.I., Elser, J.J., Haygarth, P.M., Howden, N.J.K., Jarvie, H.P., Lyu, Y., Peterson, H.M., Sharpley, Andrew N., Shen, J., Worrall, F., Zhang, F., 2016. Long-term accumulation and transport of anthropogenic phosphorus in three river basins. Nat. Geosci. 9 (5), 353–356.
Qin, H.B., Takeichi, Y., Nitani, H., Terada, Y., Takahashi, Y., 2017. Tellurium distribution and speciation in contaminated soils from abandoned mine tailings: comparison with selenium. Environ. Sci. Technol. 51 (11), 6027–6035.
Qin, H.B., Yang, S., Tanaka, M., Sanematsu, K., Arcilla, C., Takahashi, Y., 2021. Scandium immobilization by goethite: surface adsorption versus structural incorporation. Geochim. Cosmochim. Acta 294, 255–272.
Ravel, B., Newville, M., 2005. ATHENA, ARTEMIS, HEPHAESTUS: data analysis for X-ray absorption spectroscopy using IFEFFIT. J. Synchrotron Radiat. 12, 537–541.
Rodriguez, A.B., McKee, B.A., Miller, C.B., Bost, M.C., Atencio, A.N., 2020. Coastal sedimentation across North America doubled in the 20(th) century despite river dams. Nat. Commun. 11, 3249.
Rousselaki, E., Michalopoulos, P., Pavlidou, A., Kaberi, H., Prifti, E., Dassenakis, M., 2024. Pore-water nutrient concentrations variability under different oxygen regimes: a case study in Elefsis Bay, Greece. Sci. Total Environ. 915, 169830.
Rozan, T.F., Taillefert, M., Trouwborst, R.E., Glazer, B.T., Ma, S., Herszage, J., Valdes, L. M., Price, K.S., Luther Iii, G.W., 2002. Iron-sulfur-phosphorus cycling in the sediments of a shallow coastal bay: implications for sediment nutrient release and benthic macroalgal blooms. Limnol. Oceanogr. 47 (5), 1346–1354.
Rydin, E., 2000. Potentially mobile phosphorus in Lake Erken sediment. Water Res. 34, 2037–2042.
Schroth, A.W., Giles, C.D., Isles, P.D., Xu, Y., Perzan, Z., Druschel, G.K., 2015. Dynamic coupling of Iron, manganese, and phosphorus behavior in water and sediment of shallow ice-covered Eutrophic Lakes. Environ. Sci. Technol. 49 (16), 9758–9767.
Simanova, A.A., Kwon, K.D., Bone, S.E., Bargar, J.R., Refson, K., Sposito, G., Pena, J., 2015. Probing the sorption reactivity of the edge surfaces in birnessite nanoparticles using nickel(II). Geochim. Cosmochim. Acta 164, 191–204.
Smith, L., Watzin, M.C., Druschel, G., 2011. Relating sediment phosphorus mobility to seasonal and diel redox fluctuations at the sediment-water interface in a eutrophic freshwater lake. Limnol. Oceanogr. 56 (6), 2251–2264.
Song, L.T., Liu, C.Q., Wang, Z.L., Zhu, X., Teng, Y., Liang, L., Tang, S., Li, J., 2011. Iron isotope fractionation during biogeochemical cycle: information from suspended particulate matter (SPM) in Aha Lake and its tributaries, Guizhou. China. Chem. Geol. 280 (1–2), 170–179.
Tong, Y.D., Zhang, W., Wang, X., Couture, R.-M., Larssen, T., Zhao, Y., Li, J., Liang, H., Liu, X., Bu, X., He, W., Zhang, Q., Lin, Y., 2017. Decline in Chinese lake phosphorus concentration accompanied by shift in sources since 2006. Nat. Geosci. 10 (7), 507–511.
Tyrrell, T., 1999. The relative influences of nitrogen and phosphorus on oceanic primary production. Nature 400 (6744), 525–531.
Walton, C.R., Ewens, S., Coates, J.D., Blake, R.E., Planavsky, N.J., Reinhard, C., Ju, P.C., Hao, J.H., Pasek, M.A., 2023. Phosphorus availability on the early earth and the impacts of life. Nat. Geosci. 16, 399–409.
Wang, Q., Yang, P., Zhu, M.Q., 2019a. Effects of metal cations on coupled birnessite structural transformation and natural organic matter adsorption and oxidation. Geochim. Cosmochim. Acta 250, 292–310.
Wang, X., Jones, M.R., Pan, Z., Lu, X., Deng, Y., Zhu, M., Wang, Z., 2024. Trivalent manganese in dissolved forms: occurrence, speciation, reactivity and environmental geochemical impact. Water Res. 263, 122198.
Wang, Y., Ding, S.M., Gong, M., Xu, S., Xu, W., Zhang, C.S., 2016. Diffusion characteristics of agarose hydrogel used in diffusive gradients in thin films for measurements of cations and anions. Anal. Chim. Acta 945, 47–56.
Wang, Y., Ding, S.M., Ren, M.Y., Li, C., Xu, S., Sun, Q., Xu, L., 2019b. Enhanced DGT capability for measurements of multiple types of analytes using synergistic effects among different binding agents. Sci. Total Environ. 657, 446–456.
Wang, Y., Ding, S.M., Shi, L., Gong, M., Xu, S., Zhang, C.S., 2017. Simultaneous measurements of cations and anions using diffusive gradients in thin films with a ZrO-Chelex mixed binding layer. Anal. Chim. Acta 972, 1–11.
Williams, A.G.B., Scherer, M.M., 2004. Spectroscopic evidence for Fe(II)-Fe(III) electron transfer at the iron oxide-water interface. Environ. Sci. Technol. 38 (18), 4782–4790.
Wu, S., Zhao, Y., Chen, Y., Dong, X., Wang, M., Wang, G., 2019. Sulfur cycling in freshwater sediments: a cryptic driving force of iron deposition and phosphorus mobilization. Sci. Total Environ. 657, 1294–1303.
Xiong, Y., Guilbaud, R., Peacock, C.L., Cox, R.P., Canfield, D.E., Krom, M.D., Poulton, S. W., 2019. Phosphorus cycling in Lake Cadagno, Switzerland: a low sulfate euxinic ocean analogue. Geochim. Cosmochim. Acta 251, 116–135.
Xiong, Y., Guilbaud, R., Peacock, C.L., Krom, M.D., Poulton, S.W., 2023. Phosphorus controls on the formation of vivianite versus green rust under anoxic conditions. Geochim. Cosmochim. Acta 351, 139–151.
Xu, D., Chen, Y., Ding, S.M., Sun, Q., Wang, Y., Zhang, C.S., 2013. Diffusive gradients in thin films technique equipped with a mixed binding gel for simultaneous measurements of dissolved reactive phosphorus and dissolved iron. Environ. Sci. Technol. 47 (18), 10477–10484.

Yang, M., Liu, C.Q., Li, X.D., Ding, S., Cui, G., Teng, H.H., Lv, H., Wang, Y., Zhang, X., Guan, T., 2022. Carbon-sulfur coupling in a seasonally hypoxic, high-sulfate reservoir in SW China: evidence from stable CS isotopes and sulfate-reducing bacteria. Sci. Total Environ. 828, 154537.
Zerkle, A.L., Claire, M., Domagal-Goldman, S.D., Farquhar, J., Poulton, S.W., 2012. A bistable organic-rich atmosphere on the Neoarchaean earth. Nat. Geosci. 5 (5), 359–363.
Zhou, C., Gao, Y., Gaulier, C., Luo, M., Zhang, X., Bratkic, A., Davison, W., Baeyens, W., 2020. Advances in understanding mobilization processes of trace metals in marine sediments. Environ. Sci. Technol. 54 (23), 15151–15161.
Zhou, C., Gao, Y., Zhang, H., Luo, M.Y., Ma, T.H., Li, G.L., Vandeputte, D., Leermakers, M., Baeyens, W., 2024. Phosphorus mobilization in sulfidic sediments in the Baltic Sea. Sci. Total Environ. 907, 168000.
Zhu, J.Y., Song, C.Q., Wang, J.D., Ke, L.H., 2020. China's inland water dynamics: the significance of water body types. Proc. Nati. Acad. Sci. U. S. A. 117, 13876–13878.
Zhu, M.Q., Ginder-Vogel, M., Parikh, S.J., Feng, X.H., Sparks, D.L., 2010. Cation effects on the layer structure of biogenic Mn-oxides. Environ. Sci. Technol. 44 (12), 4465–4471.